Rattling mode and symmetry lowering resulting from the instability of the B_{12} molecule in LuB_{12}

N. Sluchanko,[1,2,*] A. Bogach,[1] N. Bolotina,[3] V. Glushkov,[1,2] S. Demishev,[1,2] A. Dudka,[3] V. Krasnorussky,[1] O. Khrykina,[3] K. Krasikov,[2] V. Mironov,[3] V. B. Filipov,[4] and N. Shitsevalova[4]

[1]*Prokhorov General Physics Institute, Russian Academy of Sciences, 38 Vavilov Str., 119991 Moscow, Russia*

[2]*Moscow Institute of Physics and Technology (State University), 9 Institutskiy Per., 141700 Dolgoprudny, Russia*

[3]*Shubnikov Institute of Crystallography of Federal Scientific Research Centre Crystallography and Photonics of Russian Academy of Sciences, 59 Leninskii Ave., 119333 Moscow, Russia*

[4]*Frantsevich Institute for Problems of Materials Science, National Academy of Sciences of Ukraine, 3 Krzhyzhanovsky Str., 03680 Kiev, Ukraine*

(Received 20 July 2017; revised manuscript received 20 November 2017; published 23 January 2018)

The dodecaboride LuB_{12} with cage-glass state and rattling modes has been studied to clarify the nature of the large amplitude vibrations of Lu ions. Discovered anisotropy of charge transport in conjunction with distortions of the conventional *fcc* symmetry of the crystal lattice may be attributed to coherent motion of Lu ions along a singular direction in the lattice. Arguments are presented in favor of cooperative dynamic Jahn-Teller effect in the boron sublattice to be the reason of the rattling mode, lattice distortion, and formation of the filamentary structure of the higher conducting channels—dynamic charge stripes.

DOI: 10.1103/PhysRevB.97.035150

Introduction. Rattling compounds have attracted wide interest in the last few decades due to their intriguing and exotic physical properties. Rattling effect (a large amplitude vibration of an ion in an oversized atomic cage) can be responsible for an extremely low thermal conductivity and high thermoelectric efficiency in various cage compounds, such as filled skutterudites [1], β-pyrochlore oxides [2], clathrates [3], RT_2Zn_{20} (R = Pr, La; T= Ir, Ru) [4], quadruple perovskites [5], higher borides RB_{12} [6], etc. While the rattling is usually considered as a large-amplitude localized anharmonic vibration of a single atom, recently a cluster ("collective") rattling scenario was reported [7] in $CsSnI_3$. These local excitations may also affect the electronic properties of solids due to strong electron-phonon coupling [6]. The nature of rattling motion and the mechanisms of its influence on the unusual properties and exotic ground states are still under question.

Among rattling compounds the rare earth and transition metal dodecaborides RB_{12} (R = Y, Zr, Tb-Lu) represent the simplest, model objects with face-centered cubic (*fcc*) NaCl-type crystal lattice (space group $Fm\bar{3}m$-O_h^5) built by B_{12} cuboctahedra and metal atoms R centered in the large cuboctahedral cages B_{24} formed by six neighboring B_{12} units [Figs. 1(a) and 1(b)]. Strong covalent bonds between boron atoms (both within B_{12} units and between them) form a rigid boron framework [Fig. 1(b)], which changes insignificantly in the RB_{12} family. Large difference between the size of the B_{24} cage (r(B_{24}) $\sim$ 1.1–1.15 Å, Ref. [8]), and the radius of metallic ions (0.8–0.97 Å) leads to a formation of loosely bound state of the heavy ion in the rigid B_{24} cage, resulting in low frequency (14–18 meV, Ref. [9]) dispersion-less (Einstein-like, rattling) vibrations in the phonon spectrum of dodecaborides. The electron deficiency in the boron lattice is compensated by transfer of two valence electrons ($6s^2$) from each R atom to B_{12} cluster, while the third valence electron ($5d^1$) in RB_{12} with three-valence R ions enters the conduction band. So, all rare earth dodecaborides are good metals, in which the conduction band at the Fermi level is mainly contributed from $5d$ states with a small admixture of B $2p$ electrons [10]. The only exception is a narrow-gap semiconductor YbB_{12} with exotic insulating ground state, which is observed in the regime of strong charge and spin fluctuations. Besides, YbB_{12} undergoes a metal-insulator transition at $T^* \sim 60$ K [6,8,11]. Thus, these RB_{12} rattling compounds cover a variety of ground states and the regimes of charge transport, that ranges from the unusual superconductivity (SC) in LuB_{12} and ZrB_{12} [8] and Kondo insulator (KI) [6,8,11] or topological crystalline insulator behavior [12] predicted for YbB_{12} to the complicated magnetic ordering and peculiar incommensurate magnetic structures detected for TbB_{12}-TmB_{12} antiferromagnets (AF) [8].

It is particularly important that there are some experimental evidences for the local structural distortions and boron vacancies in the cubic lattice of RB_{12} at low temperatures. It has been recently concluded [13] that these dodecaborides RB_{12} tend to form a cage-glass phase through the order-disorder phase transition (at $T^* \sim 60$ K in LuB_{12}), that results in freezing of R ions in the random positions (glass) inside the B_{24} cages with strong covalent bonds in the rigid boron sublattice (crystal). Besides, x-ray diffraction studies [14] discovered a significant tetragonal distortion of the atomic structure of LuB_{12} in the vicinity of this phase transition.

Given that LuB_{12} is a reference compound for the family of RB_{12} with a variety of ground states (AF, SC, and KI), it is important (i) to investigate an interplay between the rattling effect and features of crystalline and electronic

*nes@lt.gpi.ru

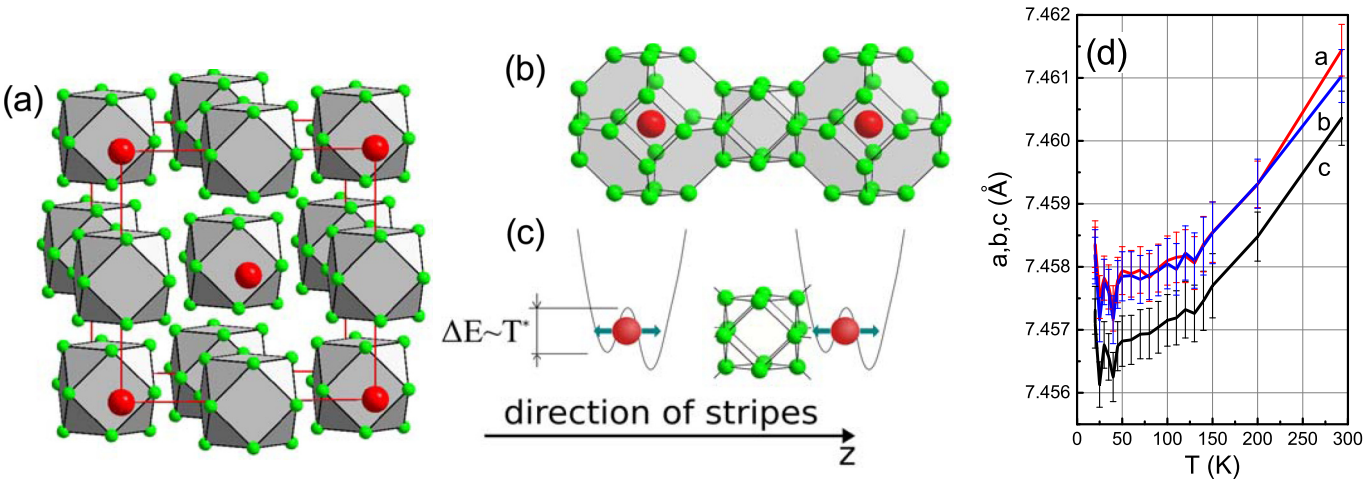

FIG. 1. (a) A NaCl-like unit cell of LuB_{12}, with Lu (red spheres) as Na and B_{12} clusters as Cl (B is shown by green spheres). (b) Two large B_{24} polyhedra centered by Lu atoms and a smaller B_{12} cuboctahedron between them. (c) Schematic view of the rattling vibrations of Lu^{3+} ions in the double-well potentials induced by the cooperative dynamic JT effect of B_{12} clusters (see text). (d) The temperature dependence of the lattice parameters a, b, and c.

structure and (ii) to shed more light on the nature of rattling in this nonmagnetic dodecaboride. Analyzing the influence of rattling mode on the transport and structural properties of LuB_{12} we studied in detail the changes of crystal structure and the anisotropy of charge carriers scattering developed at low temperatures in the cage-glass state of LuB_{12}. Then, searching for the mechanism governing the large amplitude vibration of R ion we present here the results of quantum chemical calculations and geometry optimizations for negatively charged $[B_{12}]^{2-}$ cluster. Our results argue in favor of a cooperative dynamic Jahn-Teller effect in the boron sublattice as a possible mechanism responsible for the rattling modes, structural distortions, and charge transport anisotropy in LuB_{12}. We note that these features of crystalline and electron structure of the reference compound LuB_{12} are of crucial importance both to understand unusual superconductivity (LuB_{12} and ZrB_{12}) and antiferromagnetism (TbB_{12}-TmB_{12}) and to shed light on the nature of metal-insulator transition (YbB_{12}) in the family of dodecaborides.

Experimental results. Single crystals of lutetium dodecaboride were grown by induction zone melting in an inert gas atmosphere. Structural studies were carried out on the x-ray diffractometer Xcalibur (MoKα-radiation, graphite monochromator). Precise measurements of the unit-cell parameters were done using the x-ray diffractometer Huber-5042 equipped with the enclosed-type helium cryostat [15]. Measurements of the transverse magnetoresistance were performed in a four-terminal scheme with a direct current at temperatures in the range 1.8–300 K in a magnetic field up to 80 kOe with the help of installation with a sample rotating in a magnetic field [16]. Precise x-ray diffraction reflexes [Fig. 2(a)] and quantum oscillations of the magnetization (de Haas-van Alphen effect) obtained in the orientation of the magnetic field **H**||[100] [Fig. 2(b)], testify to the high quality of crystals under investigation. Evidently, there is no one-to-one correspondence between a, b, c axes in the crystal sample measured on the x-ray diffractometer (the ball of about 0.3 mm in size) and [100], [010], [001] axes in the crystal samples (rectangular plates of about $4 \times 0.3 \times 0.3$ mm^3 in size) used for resistivity measurements.

The [010]- and [001]-elongated rectangular samples (#1 and #2 hereafter) with equally oriented (100), (010), and (001) faces were cut from one ingot of LuB_{12} [Fig. 3(a)]. The resistivity ρ(T) curves for LuB_{12} crystals #1 (measuring current **I**||[010]) and #2 (**I**||[001]), are shown [Figs. 3(c) and 3(d)] in the absence of an external magnetic field (H = 0, curves 1 and 2 correspondingly) and in steady magnetic field of 80 kOe directed along the crystal axes [100] (curve 3 for #2, curve 4 for #1), [0$\bar{1}$0] (curve 5 for #2) and [001] (curve 6 for #1). A significant anisotropy of the transverse magnetoresistance (∼20%) is observed below $T^* \sim 60$ K at $H = 80$ kOe, especially for the crystal #1 [see curves 4 and 6 in Figs. 3(c) and 3(d) for comparison], in spite of the fact that **H** directions [001] and [100] are symmetry equivalent in cubic crystals. In addition, a minimum is observed below T^* on the dependences $\rho(T, H = 80$ kOe) and the temperature lowering is accompanied with a growth of resistivity [see Figs. 3(c) and 3(d)]. Such behavior cannot be attributed to the Kondo scattering of charge carriers, because it is accompanied with a large positive magnetoresistance in these LuB_{12} crystals. Note that the resistivity $\rho(T, H = 80$ kOe) minimum below

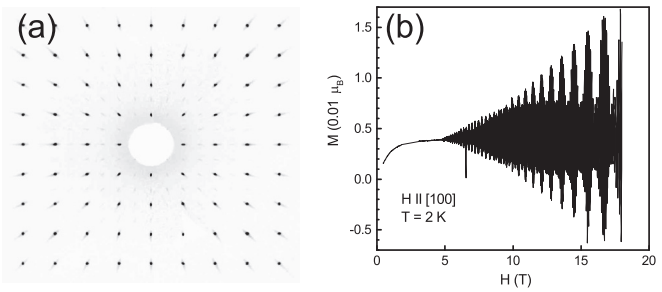

FIG. 2. (a) The $l = 0$ plane of the LuB_{12} diffraction pattern. (b) de Haas-van Alphen oscillations in LuB_{12} obtained in the orientation of the magnetic field **H**||[100].

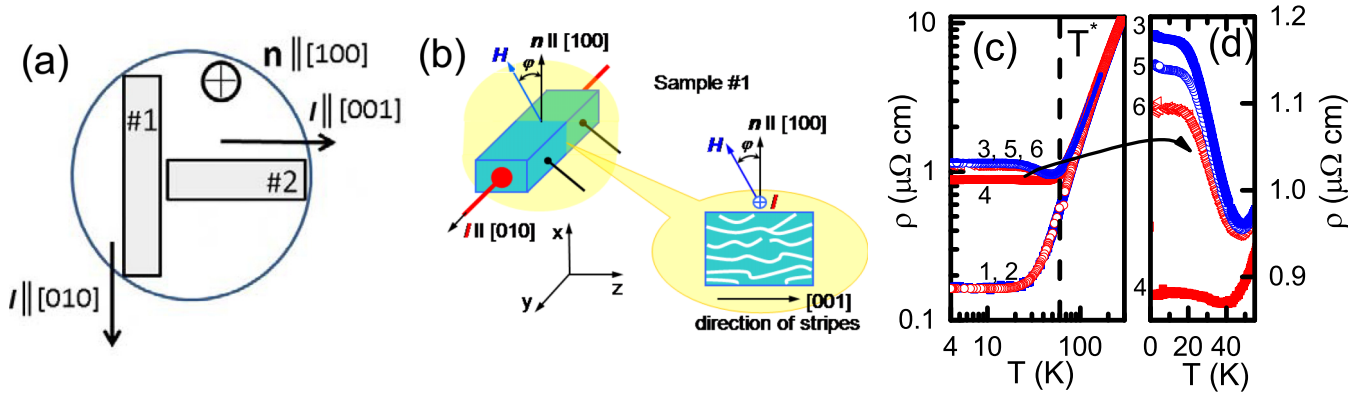

FIG. 3. (a) Two [010] and [001]-elongated rectangular samples #1 and #2 with equally oriented (100), (010), and (001) faces were cut out from one single-crystalline disk of LuB_{12} of the (100) plane. (b) Measuring scheme of transverse magnetoresistance with the sample #1 rotating about the current axis $\mathbf{I}||[010]$, φ is the angle between the normal vector $n||[100]$ and $\mathbf{H}$. Sectional drawing shows schematically the dynamic stripes (see text) directed along the z axis. The anisotropy of magnetoresistance in the sample #1 is caused by the nonequivalent $\mathbf{H}||[100]$ and $\mathbf{H}||[001]$ configurations with respect to the stripes direction [001]. (c),(d) Temperature dependences of the resistivity $\rho(T)$ for LuB_{12} crystals #1 ($\mathbf{I}||[010]$, red curves) and #2 ($\mathbf{I}||[001]$, blue curves) are shown in the absence of an external magnetic field (H = 0, curves 1,2 correspondingly) and in steady magnetic field of 80 kOe directed along the crystal axes [100] (curve 3 for #2, curve 4 for #1)), [010] (curve 5 for #2) and [001] (curve 6 for #1).

T^* is accompanied with a maximum in the vicinity of 60 K on the $R_H(T)$ curves for $\mathbf{I}||[110]$, which was detected earlier both in $Lu^N B_{12}$ with various isotopic composition in boron (N-natural, 10 and 11) [17] and in substitutional solid solutions $Zr_{1-x}Lu_xB_{12}$ [18], and this anomaly of Hall effect was associated with the transition to the cage-glass state.

To clarify the nature of the anisotropy of the transverse magnetoresistance at low temperatures, angular dependences $\rho(\varphi)$ were measured at 2–4.2 K in the magnetic fields up to 80 kOe by rotating the crystals #1 and #2 around their current axes. Families of curves $\rho_1(\varphi)$ for $\mathbf{I}||[010]$ (sample #1) and $\rho_2(\varphi)$ for $\mathbf{I}||[001]$ (sample #2) are shown in Fig. 4(a). Evidently, the angular dependences of $\rho_1(\varphi)$ do not correspond to those expected for a cubic structure. As mentioned above, the great difference is recorded for $\mathbf{H}||[\bar{1}00](\varphi = 0^\circ)$ and $\mathbf{H}||[001](\varphi = 90^\circ)$, although these directions are equivalent in cubic crystals.

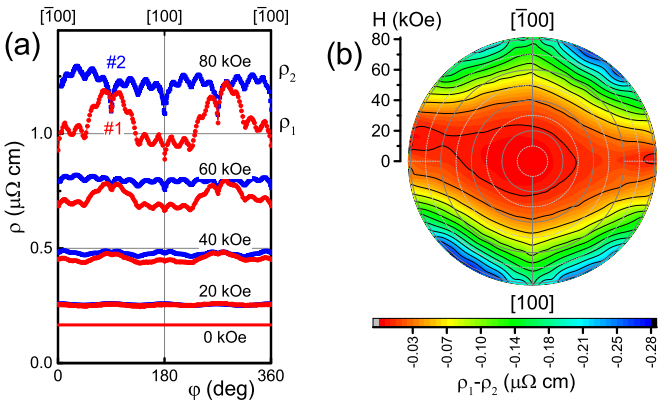

FIG. 4. (a) Angular dependences of $\rho_1(\varphi)$ and $\rho_2(\varphi)$ obtained rotating correspondingly the crystals #1 and #2 around their current axes in various magnetic fields up to 80 kOe at temperatures 2–4.2 K. (b) The anisotropy of magnetoresistance $\rho_1(\varphi) - \rho_2(\varphi) = f(\varphi, H)$ presented in the polar coordinates.

On the contrary, the sample #2 gives a set of $\rho_2(\varphi)$ singularities corresponding to practically equivalent directions [100], $[0\bar{1}0]$ (see Fig. 4(a) and Ref. [19]). The anisotropy of magnetoresistance is clearly resolved in the polar coordinates in Fig. 4(b), where the difference $\rho_1(\varphi) - \rho_2(\varphi) = f(\varphi, H)$ is presented in the colored picture. It is clearly discerned from Fig. 4(b) that conduction channels, which are transverse to the plane (001), appear in the LuB_{12} matrix.

Crystal structure. In accordance with arguments presented in Ref. [14], the *fcc* symmetry of LuB_{12} is notably distorted at low temperatures. Conventional software for the structure analysis results in calculated electron density (ED) replicating the symmetry of the structure model if even the symmetry of real ED is distorted. To provide the ability to derive probable violations of symmetry from difference Fourier maps, the crystal structure must be analyzed using a less symmetrical model (see Ref. [19] for details). Unit-cell values of LuB_{12} were refined without any symmetry restriction over the temperature range 20–300 K. Very small [$\sim$0.001 Å, see Fig. 1(d)] but steady difference of the lattice constants a,b,c was revealed, which was not accompanied by steady deviation of angular parameters from 90°. Cubic metric of the unit cell was kept, since revealed difference in the unit-cell values $c < a \cong b$ [Fig. 1(d)] was too small to influence on a result of the structure refinement. Thermal vibration of the Lu ions was described by an isotropic parameter in order that assumed anisotropy of residual ED near the Lu site could reveal itself most clearly.

Difference Fourier maps were built based on the results of the $Fmmm$ structure refinement at temperatures 90 K and 295 K (Fig. 5, see Ref. [19] for details). Each Lu site in the cubic $Fm\bar{3}m$ structure lies at the intersection of three fourfold axes perpendicular to three faces of the cubic cell. As may be seen [Figs. 5(a) and 5(b)], residual ED distribution near Lu$(0, \frac{1}{2}, \frac{1}{2})$ in the $x = 0$ face is not bound by a fourfold axis even at room temperature, which does not actually agree with $Fm\bar{3}m$.

Relief fragments of difference Fourier maps at $x = 0$ [Figs. 5(c) and 5(d)], $y = 0$ [Figs. 5(e) and 5(f)], $z = 0$

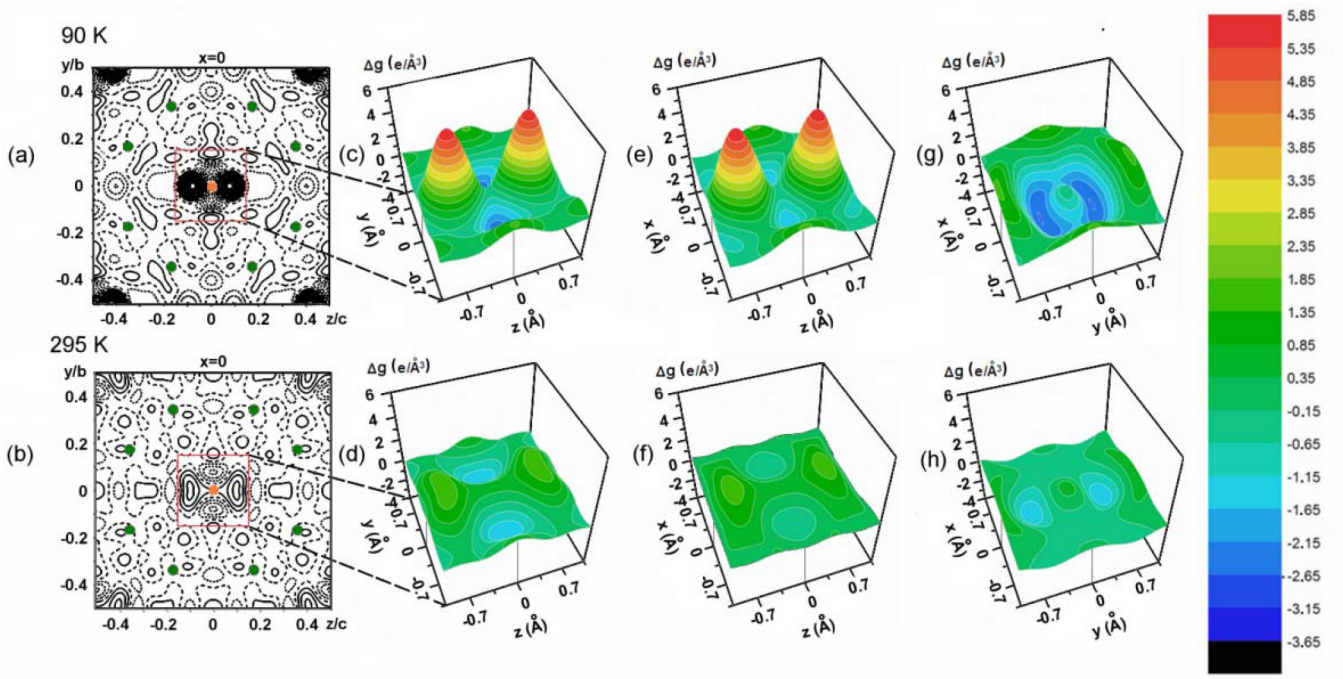

FIG. 5. Difference Fourier maps (residual ED $\Delta g, e/\text{Å}^3$) in the $x = 0$ face of the LuB_{12} unit cell at 90 K (a) and 295 K (b), respectively. Red circle is the Lu site; green circles are B sites. The (c),(d), (e),(f), and (g),(h) panels are relief drawings of difference Fourier maps made in the vicinity of the Lu ion, in the $x = 0$, $y = 0$, and $z = 0$ faces of the unit cell, whereas first and second rows of the overall picture correspond to temperatures 90 K and 295 K, respectively.

[Figs. 5(g) and 5(h)] are presented in three next columns of Fig. 5 for better visualization of residual ED distribution near the Lu site. Most notable maxima of residual ED are observed along the z axis, along which the smaller period $c \neq a \cong b$ is detected [Fig. 1(d)]. Amplitudes of residual peaks of ED increase significantly with temperature decrease being located ~0.4–0.7 Å away from a central Lu site. Taking temperature behavior of the unit-cell values into account, the character of structural distortion is closer to tetragonal. Unique z axis is not an ideal fourfold axis but can be considered as such a symmetry element to a certain approximation [19].

Discussion. To understand possible reasons for (i) the symmetry deviation of the LuB_{12} crystal from the cubic one, (ii) the significant anisotropy of the transverse magnetoresistance and the associated nonequivalence of the directions **H**||[001] and **H**||[100] in the charge carriers scattering [Figs. 3(c), 3(d), 4, and Ref. [19]], and (iii) the growth of resistance with the temperature lowering in a steady magnetic field [Figs. 3(c) and 3(d)], we discuss herein a possible scenario associated with the Jahn-Teller (JT) effect. More specifically, because of triple orbital degeneracy of the ground electronic state, the B_{12} molecules are JT active and thus their structure is labile due to JT distortions. In this case, upon decreasing temperature, some intrinsic structural defects (such as boron vacancies and mixed ^{10}B-^{11}B isotope composition of B_{12} molecules) can lift degeneracy due to symmetry lowering and may cause an electronic phase transition associated with JT structural instability. Similar phase transformations produced by JT effect of B_{12} icosahedra were earlier observed in higher borides [20].

In order to establish the amplitude and type of the JT distortions in B_{12} cuboctahedra, we performed quantum chemical calculations and geometry optimizations for charged $[B_{12}]^{2-}$ cluster, whose doubly negative charge state is regarded as the most relevant in RB_{12} compounds (see Ref. [19]). The structure is shown in Fig. 6. Interestingly, the actual symmetry of the JT distorted cluster (C_{2h}) is lower than the symmetry of tetragonal (D_{4h}) and trigonal (D_{3d}) JT minima expected from the JT theory [21]. The amplitude of the JT distortions of isolated B_{12} clusters is rather pronounced as the bond lengths and bonding angles can vary by ~0.1 Å and ~5°, respectively (Fig. 6 and Ref. [19]).

These results provide evidence that the JT structural liability of B_{12} clusters should play an important role in the microscopic mechanism of lattice distortions of LuB_{12} at low temperatures. Taking into account that B_{12} clusters form an extended 3D covalent network, being connected by B-B covalent bonds, one can suggest that structural JT liability should retain and reinforce in the boron sublattice of the dodecaborides. The reinforcement due to cooperative dynamic JT effect manifested both in static and dynamic lattice properties may be considered as the cause of large amplitude displacements of Lu atoms in oversized B_{24} cages, resulting in quasitetragonal distortions of the *fcc* lattice and the anisotropy of magnetoresistance in LuB_{12} at low temperatures. Therefore, the rattling modes can be attributed to quantum motion of the Lu ions in the double-well potentials (DWPs) with the minima displaced from each other for a distance of 0.4–0.7 Å along the z axis [see Figs. 5(c) and 5(e)]. The barrier height $\Delta E = 51$–$97K$ in DWP is detected [22] for LuB_{12} with different numbers of boron vacancies and Zr impurities. Concentration of Lu ions displaced from centres in B_{24} cuboctahedra is estimated to be 3–8 at.%. This agrees well with the 3.6 at.% concentration

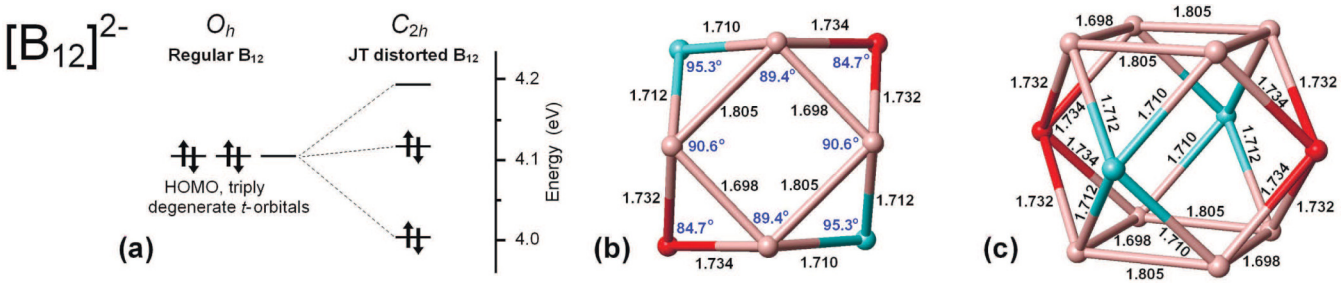

FIG. 6. (a) JT splitting of triply degenerate highest occupied molecular orbital with four electrons is indicated. Molecular structure of isolated cluster $[B_{12}]^{2-}$ in the local JT energy minimum as obtained from DFT geometry optimization calculations [19] [projection (b) and perspective view (c)]. Principal atomic distances (Å) and bond angles are indicated. The structure exhibits the C_{2h} symmetry. There are three groups of equivalent (symmetry related) boron atoms shown as pink, red, and blue balls.

of the off-site Lu ions obtained from the EXAFS measurements at low temperatures [23], where Lu displacements by 0.2–0.3 Å are established. These large amplitude vibrations of heavy ions in DWP are shown schematically in Fig. 1(c), and as a sequence of the Lu-ions quantum motion (zero temperature vibrations) the dramatic changes of the $5d-2p$ hybridization of electron states should be expected along the unique z axis. It results in formation of higher conductive channels—dynamic charge stripes [24] with a strong charge carrier scattering on the filamentary structure in the LuB_{12} *fcc* matrix.

Note that the case is different from charge density wave electronic instability. Indeed, the charge modulation due to stripe formation is not directly related to Fermi surface nesting but results from electronic correlations and/or strong electron-phonon interaction. Periodic charge density modulation, which forms as a result of stripe formation, induces a periodic distortion of the crystal lattice with the same propagation vector. Its magnitude is proportional to the electron-phonon coupling strength. Such distortions have been observed, for instance, by neutron diffraction and scanning tunneling microscopy in a number of oxide perovskites as well as some other systems (see, for example, references in the review papers [24,25]). Recently, the results of direct measurement of dynamic charge stripes by inelastic neutron scattering have been reported for $La_{2x}Sr_xNiO_4$ [26].

Thus, the presence of charge stripe order should, through striction, cause the lattice parameters parallel and perpendicular to the stripes to become inequivalent, and this effect was certainly detected in our measurements of the lattice parameters a, b, and c in LuB_{12} [see Fig. 1(d)]. Charge density fluctuations associated with dynamic stripes may soften and/or broaden certain phonons signaling an incipient lattice instability [24], in correlation with emergence of dispersionless vibrations in the phonon spectrum [9] and appearance of Boson peak [13,27] in the cage-glass state of dodecaborides. Following to Ref. [25] it is worth noting here that (i) from the strong coupling perspective charge stripes are a real-space pattern of micro phase separation and (ii) the microscopic mechanism of stripe formation in particular materials is still not clear. So, our interpretation of the electronic instability in terms of the cooperative dynamic Jahn-Teller effect in the boron sublattice may be considered as one of the possible scenario of charge stripe formation in metallic systems.

We suppose that some fine structure observed on the resistivity angular dependencies with an oscillated behavior of $\rho_{1,2}(\varphi)$ may be also explained in terms of scattering of charge carriers on the dynamic stripes. The period of these oscillations changes in the range 20–27° and these features are very similar for crystals #1 and #2 under investigations [see Fig. 4(a)]. Unfortunately, there is at present no appropriate theory to describe the charge carriers scattering on dynamic stripes in metals, so new theoretical and experimental work is necessary to understand the interplay between the electronic instability and charge transport in LuB_{12}.

Conclusion. Lutetium dodecaboride has been studied here as the model rattling compound to clarify the nature of rattling modes and their influence on the crystal structure and properties. Precision measurements of the crystal structure and charge transport at low temperatures allow detecting the symmetry lowering, which may be attributed to coherent quasilocal vibrations (rattling modes) of Lu ions along a singular direction in the dodecaboride lattice. It has also been shown that there is an extra source of lattice instability in LuB_{12} related to the Jahn-Teller effect of B_{12} clusters, which can manifest in concert with displacements of Lu atoms in oversized B_{24} cages resulting in cooperative dynamic Jahn-Teller lattice distortions and conduction band changes.

Acknowledgments. This work was supported by grants from RFBR (Russia), 15-02-02553, 16-02-00171. The structure measurements were performed using the equipment of the Shared Research Center FSRC Crystallography and Photonics RAS. One of us (N.S.) acknowledges V. Moshchalkov and F. Antson for useful discussions.

[1] V. Keppens, D. Mandrus, B. Sales, B. Chakoumakos, P. Dai, R. Coldea, M. Maple, D. Gajewski, E. Freeman, and S. Bennington, Nature (London) **395**, 876 (1998); Y. Nakai, K. Ishida, H. Sugawara, D. Kikuchi, and H. Sato, Phys. Rev. B **77**, 041101 (2008).

[2] M. Yoshida, K. Arai, R. Kaido, M. Takigawa, S. Yonezawa, Y. Muraoka, and Z. Hiroi, Phys. Rev. Lett. **98**, 197002 (2007).

[3] G. S. Nolas, J. L. Cohn, G. A. Slack, and S. B. Schujman, Appl. Phys. Lett. **73**, 178 (1998); S. Paschen, M. Ikeda, S. Stefanoski, and G. Nolas, in *The Physics and Chemistry of*

Inorganic Clathrates, Springer Series in Materials Science, Vol. 199, edited by G. Nolas (Springer, Netherlands, 2014), Chap. 9, pp. 249–276.

[4] K. Asaki, H. Kotegawa, H. Tou, T. Onimaru, K. Matsumoto, Y. Inoue, and T. Takabatake, J. Phys. Soc. Jpn. **81**, 023711 (2012).

[5] Y. Akizuki, I. Yamada, K. Fujita, K. Taga, T. Kawakami, M. Mizumaki, and K. Tanaka, Angew. Chem. Int. Ed. **54**, 10870 (2015).

[6] N. E. Sluchanko, A. V. Bogach, V. V. Glushkov, S. V. Demishev, K. S. Lyubshov, D. N. Sluchanko, A. V. Levchenko, A. B. Dukhnenko, V. B. Filipov, S. Gabani, and K. Flachbart, JETP Lett. **89**, 256 (2009); P. A. Alekseev, K. S. Nemkovski, J.-M. Mignot, E. S. Clementyev, A. S. Ivanov, S. Rols, R. I. Bewley, V. B. Filipov, and N. Y. Shitsevalova, Phys. Rev. B **89**, 115121 (2014).

[7] W. Lee, H. Li, A. B. Wong, D. Zhang, M. Lai, Y. Yu, Q. Kong, E. Lin, J. J. Urban, J. C. Grossman, and P. Yang, Proc. Natl. Acad. Sci. **114**, 8693 (2017).

[8] P. Alekseev, G. Grechnev, N. Shitsevalova, K. Siemensmeyer, N. Sluchanko, O. Zogal, and K. Flachbart, in *Rare Earths: Research and Applications*, edited by K. Delfrey (Nova, Commack, New York, 2008), Chap. 2, p. 79.

[9] A. V. Rybina, K. S. Nemkovski, P. A. Alekseev, J.-M. Mignot, E. S. Clementyev, M. Johnson, L. Capogna, A. V. Dukhnenko, A. B. Lyashenko, and V. B. Filippov, Phys. Rev. B **82**, 024302 (2010).

[10] M. Heinecke, K. Winzer, J. Noffke, H. Kranefeld, H. Grieb, K. Flachbart, and Y. B. Paderno, Z. Phys. B **98**, 231 (1995); B. Jager, S. Paluch, O. J. Zogał, W. Wolf, P. Herzig, V. B. Filippov, N. Y. Shitsevalova, and Y. B. Paderno, J. Phys. Condens. Matter **18**, 2525 (2006).

[11] J.-M. Mignot, P. A. Alekseev, K. S. Nemkovski, L.-P. Regnault, F. Iga, and T. Takabatake, Phys. Rev. Lett. **94**, 247204 (2005).

[12] H. Weng, J. Zhao, Z. Wang, Z. Fang, and X. Dai, Phys. Rev. Lett. **112**, 016403 (2014).

[13] N. E. Sluchanko, A. N. Azarevich, A. V. Bogach, I. I. Vlasov, V. V. Glushkov, S. V. Demishev, A. A. Maksimov, I. I. Tartakovskii, E. V. Filatov, K. Flachbart, S. Gabani, V. B. Filippov, N. Yu. Shitsevalova, and V. V. Moshchalkov, Zh. Eksp. Teor. Fiz. **140**, 536 (2011) [J. Exp. Theor. Phys. **113**, 468 (2011)].

[14] N. B. Bolotina, I. A. Verin, N. Y. Shitsevalova, V. B. Filippov, and N. E. Sluchanko, Crystallogr. Rep. **61**, 181 (2016).

[15] A. P. Dudka, I. A. Verin, and A. M. Antipin, Crystallogr. Rep. **60**, 316 (2015).

[16] I. I. Lobanova, V. V. Glushkov, N. E. Sluchanko, and S. V. Demishev, Sci. Rep. **6**, 22101 (2016).

[17] N. E. Sluchanko, A. N. Azarevich, A. V. Bogach, V. V. Glushkov, S. V. Demishev, A. V. Kuznetsov, K. S. Lyubshov, V. B. Filippov, and N. Yu. Shitsevalova, Zh. Eksp. Teor. Fiz. **138**, 315 (2010) [J. Exp. Theor. Phys. **111**, 279 (2010)].

[18] N. E. Sluchanko, A. N. Azarevich, M. A. Anisimov, A. V. Bogach, S. Y. Gavrilkin, M. I. Gilmanov, V. V. Glushkov, S. V. Demishev, A. L. Khoroshilov, A. V. Dukhnenko, K. V. Mitsen, N. Y. Shitsevalova, V. B. Filipov, V. V. Voronov, and K. Flachbart, Phys. Rev. B **93**, 085130 (2016).

[19] See Supplemental Material at http://link.aps.org/supplemental/10.1103/PhysRevB.97.035150 for more information: The illustration of a symmetry lowering in LuB_{12}: X-ray data are collected at $T = 140$ K and difference Fourier maps are obtained when structural symmetry is described using $Fm\bar{3}m$ (a)–(c) and $Fmmm$ (d)–(f) groups (Fig. S1). In depth information on magnetoresistance as obtained for samples #1 and #2 (Fig. S2). The results of quantum chemical calculations for electrically neutral $[B_{12}]^0$ and negatively charged clusters $[B_{12}]^{n-}$ ($n = 1 - 4$) with detailed discussion (Fig. S3).

[20] R. Franz and H. Werheit, Europhys. Lett **9**, 145 (1989).

[21] I. B. Bersuker and V. Z. Polinger, *Vibronic Interactions in Molecules and Crystals* (Springer, Berlin, 1989).

[22] N. E. Sluchanko, A. N. Azarevich, S. Gavrilkin, V. V. Glushkov, S. V. Demishev, N. Y. Shitsevalova, and V. B. Filipov, JETP Lett. **98**, 578 (2014).

[23] A. P. Menushenkov, A. A. Yaroslavtsev, I. A. Zaluzhnyy, A. V. Kuznetsov, R. V. Chernikov, N. Y. Shitsevalova, and V. B. Filippov, JETP Lett. **98**, 165 (2013).

[24] D. Reznik, Physica C: Superconductivity **481**, 75 (2012).

[25] S. A. Kivelson, I. P. Bindloss, E. Fradkin, V. Oganesyan, J. M. Tranquada, A. Kapitulnik, and C. Howald, Rev. Mod. Phys. **75**, 1201 (2003).

[26] S. Anissimova, D. Parshall, G. Gu, K. Marty, M. D. Lumsden, S. Chi, J. A. Fernandez-Baca, D. Abernathy, D. Lamago, J. M. Tranquada, and D. Reznik, Nat. Commun. **5**, 3467 (2014).

[27] N. E. Sluchanko, A. Azarevich, M. Anisimov, A. V. Bogach, S. Y. Gavrilkin, V. V. Glushkov, S. V. Demishev, A. A. Maksimov, I. I. Tartakovskii, E. Filatov *et al.*, JETP Lett. **103**, 674 (2016).